LETTERS
https://doi.org/10.1038/s41558-018-0248-0
nature climate change

Cross-equatorial winds control El Niño diversity and change

Shineng Hu[1,2*] and Alexey V. Fedorov[1]

Over the past two decades, El Niño events have weakened on average and their sea surface temperature (SST) anomalies shifted westward towards the central Pacific. Moreover, the intertropical convergence zone (ITCZ), which typically migrates southward from its northerly position during El Niño events, has not crossed the Equator since 1998. The causes of these changes remain under debate[1–5]. Here, using in situ, satellite and atmospheric reanalysis data, we show they can be related to a multidecadal strengthening of cross-equatorial winds in the eastern Pacific. This gradual strengthening of meridional winds is unlikely to be caused by El Niño/Southern Oscillation (ENSO) changes, and contains signals forced both locally and from outside the tropical Pacific, probably from the tropical North Atlantic. Coupled model simulations in which the observed cross-equatorial wind strengthening is superimposed successfully reproduce the key features of the recent changes in tropical climate. In particular, the tropical mean state experiences a 'La Niña-like' change, the ENSO amplitude weakens by about 20%, the centre of the SST anomalies shifts westward and the ITCZ now rarely crosses the Equator. Thus, cross-equatorial winds are found to modulate tropical Pacific mean state and variability, with implications for quantifying projected changes in ENSO under anthropogenic warming.

El Niño, the warm phase of a quasi-periodic oscillation that results from tropical ocean–atmosphere interactions in the Pacific, has strong impacts on global climate, but how this phenomenon should change with anthropogenic warming is still debated, despite ongoing research[6–12]. In fact, the tropical Pacific has experienced a relatively quiet period of El Niño activity since the 1997 extreme event, until another extreme El Niño developed in 2015–2016. This followed the weak 2014 warm event[13] and began after a strong sequence of westerly wind bursts[14–16]. Despite its large magnitude, the 2015 event exhibited several features distinct from the previous 1982 and 1997 strong events (Fig. 1a,b). Specifically, the maximum SST anomaly did not reach the coast of Peru in 2015, and the eastern Pacific ITCZ failed to cross the Equator even at the El Niño peak. In fact, these features are more common for weak central Pacific (CP) El Niño events, but are in sharp contrast to Eastern Pacific (EP) El Niño events that dominated two decades earlier[2,3,5] (Fig. 1c). The ITCZ precipitation band, whose mean climatological position is north of the Equator, would typically migrate towards the Equator during a strong EP El Niño, but not so during CP El Niño (Supplementary Fig. 1). Other terminologies for CP and EP El Niño are also used[1,3]. Although the 2015–2016 El Niño is considered an EP event based on the warming magnitude in the eastern Pacific[14,15], it shared properties of both types throughout its development[15,17].

The weaker activity of El Niño and the impeded southward migration of the ITCZ reflect a substantial change in ENSO variability. The ENSO signal weakened, especially in the eastern equatorial Pacific, with about a 20% reduction over several decades (Fig. 1e). Concurrently, the tropical Pacific experienced a negative phase of the Interdecadal Pacific Oscillation[18], characterized by a broad cooling in the eastern tropical Pacific and stronger trade winds (Fig. 1d). These 'La Niña-like mean state changes and the ENSO weakening may be connected[5], but which one causes the other remains unclear[19]. Moreover, whether these ENSO changes are externally forced, as investigated in this study, or reflect internal variability cannot be assessed solely based on the relatively short observational records[20].

Another important aspect of the mean state changes, largely overlooked before and the main focus of this study, is decadal anomalies in southerly winds that extend from the southeastern to the northeastern subtropical Pacific (Fig. 1d). These cross-equatorial wind anomalies are not part of the Interdecadal Pacific Oscillation pattern, which is largely symmetric with respect to the Equator.

The climatological cross-equatorial winds, a salient feature of the eastern Pacific, are associated with a northward-displaced ITCZ and a strong meridional SST gradient maintained by the wind–evaporation–SST feedback[21]. The strengthening of these winds, observed across different data sets (Supplementary Fig. 2), is statistically significant ($P<0.01$ (Supplementary Fig. 3)) and gives a surface expression of an accelerated atmospheric shallow that overturns circulation within 10° S to 10° N below 500 hPa (Supplementary Fig. 4).

The cross-equatorial winds undergo interannual variations such that they typically vanish when a strong El Niño occurs (for example, the 1997 and 1982 events), but show little connection to weak El Niño events or La Niña (Fig. 2a). Nevertheless, these winds remained persistently strong during the extreme El Niño in 2015 (Fig. 2a), consistent with the ITCZ staying north of the Equator during this event (Fig. 1a). Here we will argue that these particular characteristics of the 2015 event are dynamically connected to the multidecadal strengthening of cross-equatorial winds.

To examine trends and variability of cross-equatorial winds quantitatively, we compute a monthly wind index, V_{EP}, by averaging the meridional surface wind anomalies in the eastern equatorial Pacific, and compared it to other temperature indices (Methods). As already mentioned, V_{EP} is only weakly modulated by the ENSO cycle ($r=-0.33$ (Fig. 2b)). This suggests that the eastern Pacific cross-equatorial wind anomalies are not likely to be directly forced by ENSO.

Rather, V_{EP} is tightly connected to the local meridional SST gradient in the eastern equatorial Pacific ($r=0.83$ (Fig. 2c)). Nevertheless, based on linear regression, this local SST gradient can only explain

[1]Department of Geology and Geophysics, Yale University, New Haven, CT, USA. [2]Present address: Scripps Institution of Oceanography, University of California, San Diego, CA, USA. *e-mail: shineng.hu@gmail.com

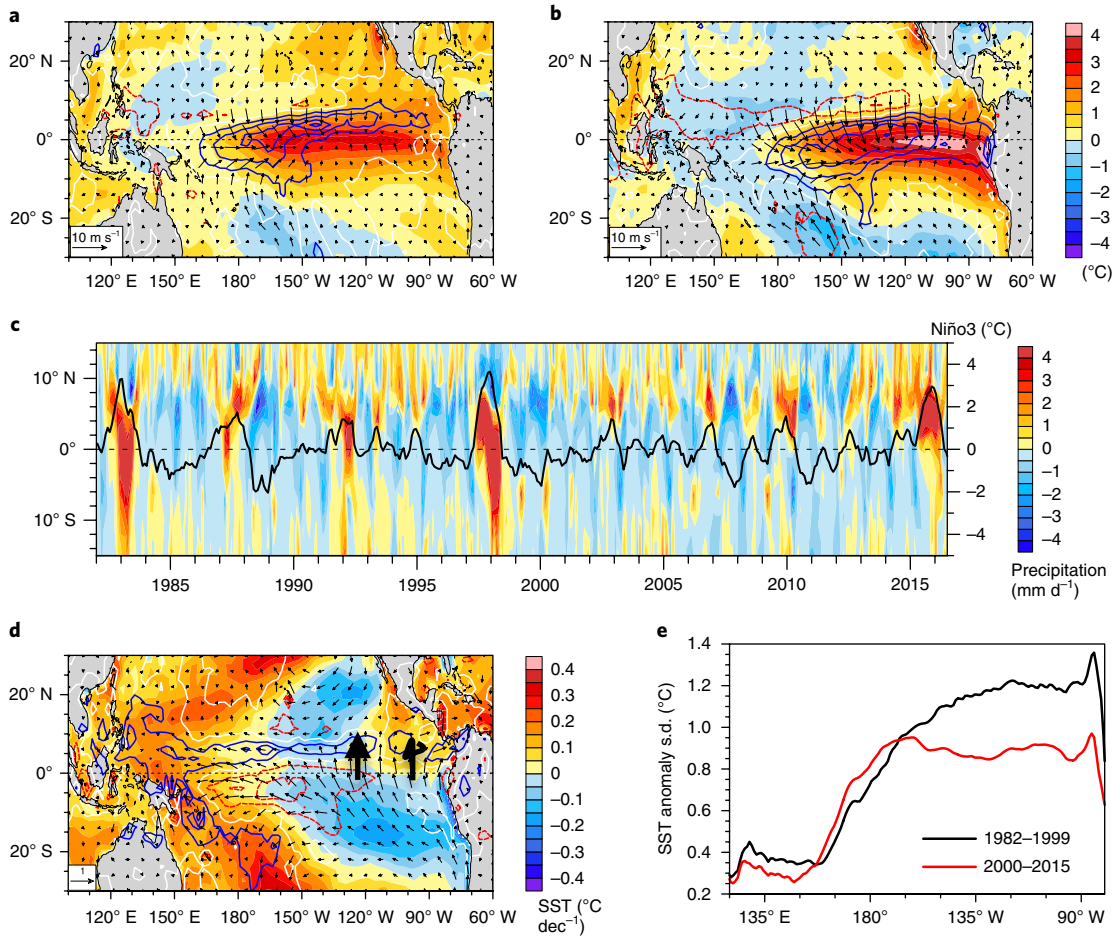

Fig. 1 | Observed multidecadal changes in tropical Pacific mean state and ENSO. a,b October–March mean SST, surface winds (arrows) and precipitation (contours at 3 mm d^{-1} intervals) anomalies at the peak of the extreme El Niño of 2015–2016 (**a**) and 1997–1998 (**b**). **c**, A Hovmoller diagram for the eastern Pacific precipitation anomalies averaged within 150–90° W, overlaid with Niño3 variations (black line). **d**, Multidecadal trends in SST, surface winds (arrows (m s^{-1} dec^{-1})), and precipitation (contours at 0.25 mm d^{-1} dec^{-1} intervals) over the period 1982–2015. For the precipitation anomalies, blue, red and white contours indicate positive, negative and zero values, respectively. **e**, Standard deviations of equatorial (5° S to 5° N) SST anomalies during 1982–1999 and 2000–2015.

about half of the multidecadal trend in V_{EP} (0.11 out of 0.22 m s^{-1} dec^{-1}). The rest of the wind signal, termed $V_{EP\text{-residual}}$, contains the other half of the trend (0.11 m s^{-1} dec^{-1} (Fig. 2d)) and should include any contribution induced from outside the tropical Pacific.

What causes this remote component of the cross-equatorial wind strengthening? The concurrent warming of the tropical North Atlantic[22], as part of the positive phase of the Atlantic Multidecadal Oscillation (AMO)[23], could provide such a contribution (r=0.58 (Fig. 2d)). Our additional coupled climate simulations suggest that the tropical North Atlantic warming could, indeed, explain a trend of about 0.15 m s^{-1} dec^{-1}, that is, about two-thirds of the observed trend (Methods and Supplementary Fig. 5). A faster warming of the Northern Hemisphere than the Southern Hemisphere may also induce a stronger cross-equatorial flow[24,25]. However, our additional slab–ocean simulations that imposed the observed interhemispheric asymmetry in SST trends show only a weak signal in the equatorial Pacific. Further research is needed to have a more definite attribution and to determine whether the meridional wind strengthening is externally forced or internally generated.

The reduction of ENSO variance, as measured along the Equator, occurred within a similar longitudinal range as the intensification of the cross-equatorial winds, which suggests a possible link between the two (Fig. 1d,e). As the cross-equatorial wind strengthening is unlikely to be directly induced by ENSO changes, as shown above, we therefore explored the dynamical impacts of the cross-equatorial wind strengthening on the ENSO variability and tropical Pacific mean state.

We conducted two sets of coupled climate simulations (control and perturbed), each integrated for over 500 years to detect robust changes in ENSO[20]. Current state-of-the-art general circulation models (GCMs), which include the Community Earth System Model (CESM) used in this study, typically have strong SST and precipitation biases in the tropical mean state[26], especially when seasonal cycle is considered (Supplementary Figs. 6 and 7). They include the so-called double ITCZ problem[26], which strongly affects cross-equatorial winds. To avoid the potential impacts of such background model biases on ENSO simulations, we first corrected the tropical Pacific mean state SST bias in CESM by applying seasonally varying surface heat flux anomalies (Methods), which greatly improved the model representation of the ITCZ and cross-equatorial winds (Supplementary Figs. 6 and 7). This corrected simulation has a realistic representation of ENSO (Supplementary Fig. 7) and was used as the control experiment (CTL). Within the perturbed simulation (CrE), we added cross-equatorial wind stress anomalies, equivalent to three decades of the observed trend (Fig. 3a), to wind produced by the coupled model. The difference between the two simulations was then assessed.

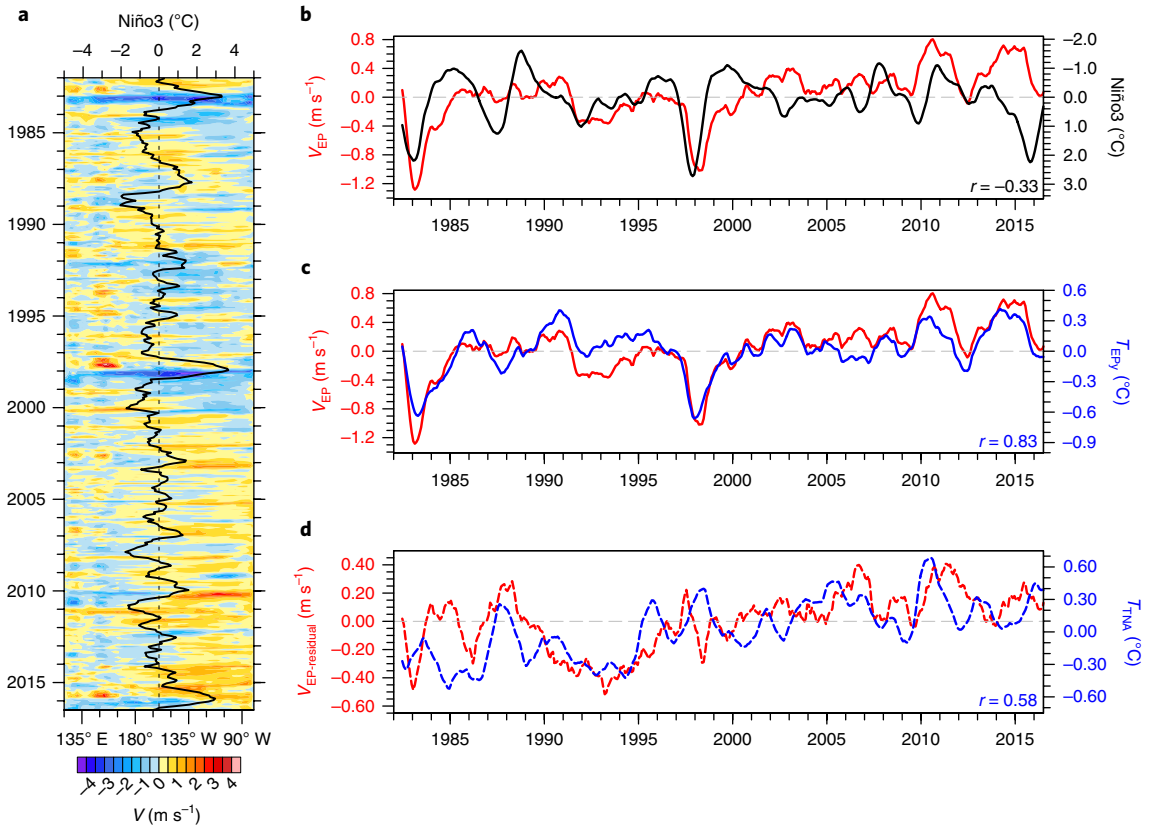

Fig. 2 | Observed trends and variations in cross-equatorial winds. a, A Hovmoller diagram for cross-equatorial wind anomalies averaged within 5° S to 5° N overlaid with Niño3 variations (black line). **b**,**c**, Variations in the eastern Pacific cross-equatorial wind index (red line) versus the Niño3 index (black line) (**b**) and the eastern Pacific meridional SST gradient (blue line) (**c**) . **d**, The remotely forced component of cross-equatorial wind (dashed red line) and the SST variations in the tropical North Atlantic (0–30° N) (dashed blue line). Methods gives the detailed definitions. In **b**–**d**, the time series are smoothed by applying an 11-month running mean, and the cross-correlation coefficient *r* is shown at the bottom-right corner of each panel.

The superimposition of the cross-equatorial wind stress anomalies induced westward anomalies in the zonal flow near 5° S and eastward anomalies near 5° N due to the Ekman effect; the westward flow penetrated further into the Northern Hemisphere due to momentum advection by the mean cross-equatorial northward ocean flow[27] (Supplementary Fig. 8). The anomalous horizontal advection induced by these ocean current changes, in turn, led to a strong cooling south of the Equator and a slight warming to the north (Fig. 3b). The northward wind stress near Peru generated a strong local cooling via coastal upwelling, which was then transported westward via advection and Rossby waves, and contributed to the meridional SST asymmetry[27].

The anomalous meridional SST gradient across the Equator further strengthens the cross-equatorial winds as a coupled model response, by about 30% with respect to the superimposed winds, but only within the equatorial band (10° S to 10° N), which amplifies the SST response through the wind–evaporation–SST feedback[21] (Fig. 3b). The induced changes in SST and winds lead to an ITCZ response quite similar to the observed trend; it includes the ITCZ intensification along 5° N and the drying over the central–eastern equatorial Pacific south of the ITCZ (Fig. 3b (and also Fig. 1d)).

In addition to the mean state changes, superimposing cross-equatorial wind anomalies also led to a pronounced reduction in ENSO variability, especially to the east of the dateline (Fig. 3c). Consequently, the variability of Niño3 (the SST anomalies averaged within 5° S to 5° N and 150–90° W) is reduced by 17% (Fig. 3d), and the active region of interannual SST variations along the Equator moves westward, which implies a shift from EP to CP events within the El Niño continuum (Methods and Supplementary Fig. 9). In fact, the ratio of the number of CP events to EP events is 1.2 for the CTL run (55% are CP events and 45% are EP events), which increases to 1.8 for the CrE run (64% CP versus 36% EP (Methods)). All these changes are consistent with the observations over the past decades (Fig. 1e). The probability of extreme El Niño events decreases by about 40–60%, depending on whether extreme events are defined via SST[15] or precipitation[9] (Fig. 3e,f). The reduction in strong precipitation events in the eastern equatorial Pacific (Fig. 3f), arguably related to colder mean SSTs that make it harder for El Niño precipitation to pass the convective threshold[9], implies that the ITCZ crosses the Equator less frequently, also consistent with the observations (Fig. 1c). Our additional coupled simulation with an imposed tropical North Atlantic warming, which generates strong cross-equatorial winds in the Pacific, shows consistent results in ENSO reduction (Supplementary Fig. 5).

What are the mechanisms of the weakening of ENSO variability? We conducted a heat budget analysis[3,17] of the mixed-layer ocean temperature averaged over the Niño3 box within the upper 50 m during the El Niño development phase. All the major positive terms that affect temperature were reduced (Supplementary Fig. 10), including those responsible for the main positive feedbacks: (1) meridional advection feedback ($\bar{v}T'_y$), (2) thermocline feedback ($\bar{w}T'_z$), (3) Ekman feedback ($w'\bar{T}_z$) and (4) zonal advection feedback ($u'\bar{T}_x$), where T is the ocean potential temperature, u, v and w are the zonal, meridional and vertical currents, bars show climatological means and primes indicate anomalies with respect to the model climatology. The reduction of these four terms between CTL and CrE is consistent with the weaker ENSO feedbacks since 2000 found by other authors[28]. In our simulation, it is caused mainly by mean state

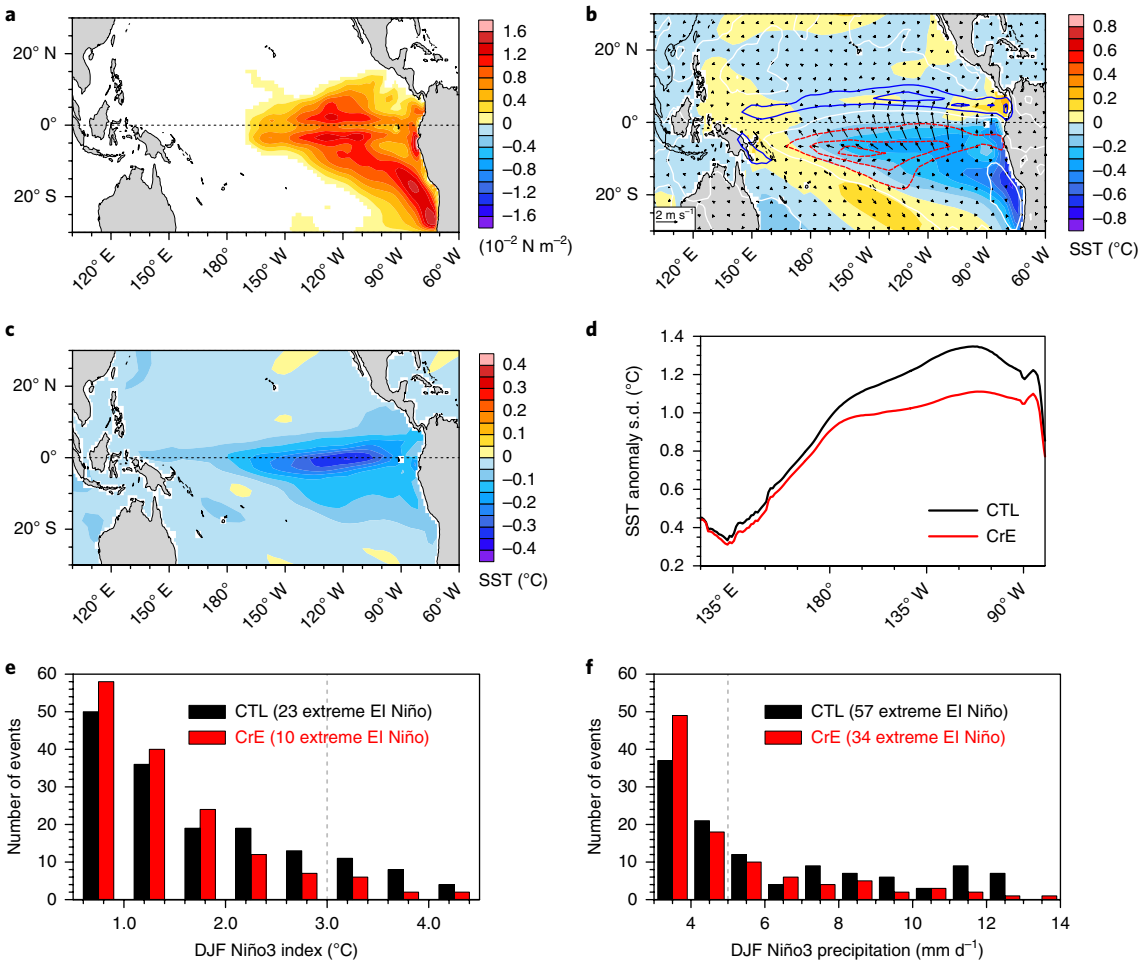

Fig. 3 | Coupled model response to the superimposed cross-equatorial wind anomaly. a, Meridional wind stress anomaly added within the CrE simulation. **b**, Differences between the CrE and CTL simulations in SST, surface winds (arrows) and precipitation (contours at 0.4 mm d^{-1} intervals). Blue, red and white contours indicate positive, negative and zero values, respectively. **c,** Differences between CrE and CTL in standard deviations of the SST anomalies. **d**, Standard deviations of equatorial (5° S to 5° N) SST anomalies for CTL and CrE. **e**,**f**, Histograms for the numbers of warm events per 500 years in each simulation for the December–February (DJF) Niño3 index (**e**) and the DJF Niño3 precipitation (**f**). The vertical dashed lines mark the thresholds for extreme El Niño.

changes associated with (1) stronger northward cross-equatorial currents that advect temperature anomalies off the equatorial band, (2) a weaker sensitivity of the mixed-layer temperature to thermocline variations (that is, deeper mean thermocline), (3) a weaker mean vertical thermal stratification and (4) a weaker mean zonal temperature contrast, respectively (Supplementary Fig. 11). Although, formally, such feedback terms could become smaller simply because of weaker El Niño composites, the reduction of the meridional advection feedback ($\bar{v}T'_y$) yields the largest contribution, which confirms its importance for the ENSO amplitude. Our results are consistent with previous studies that looked at the role of the seasonality of cross-equatorial winds in ENSO[29,30].

Thus, our study highlights the important role of cross-equatorial winds in the tropical Pacific climate mean state and variability, in addition to the role of zonal wind discussed in previous studies[4,5,18], and suggests that changes in these winds should be monitored. Potential factors that may affect the magnitude of Pacific cross-equatorial winds in the future include SST anomalies in the tropical North Atlantic associated with changes in the phase of the Atlantic Multidecadal Oscillation[22,23] and/or the state of the Atlantic Multidecadal Oscillation Circulation[31–33], and the interhemispheric asymmetry in anthropogenic warming[34] due to, for example, aerosols or land mass distributions. Under anthropogenic global warming, the slowdown of the Atlantic Multidecadal Oscillation Circulation[31–33] may weaken the cross-equatorial winds by cooling the tropical North Atlantic, whereas the reduction of anthropogenic aerosols primarily in the Northern Hemisphere[35] tends to intensify those winds.

We emphasize that our study focuses mainly on the impacts of cross-equatorial winds on the ENSO variability on multidecadal timescales, but the role that interannual variations in these winds play in a particular El Niño event needs further investigation. For example, during the 1982/1983 and 1997/1998 events, the weakening of cross-equatorial winds might have provided a positive feedback to El Niño development.

Finally, future changes in cross-equatorial winds remain highly uncertain (Fig. 4) because the relative contribution of the competing factors mentioned above depends on the model and climate scenario used and is strongly affected by the model double-ITCZ problem[26]. At present, most climate models severely underestimate these winds (Fig. 4). Consequently, all these factors should be carefully assessed to understand the changes in cross-equatorial winds and how they may affect ENSO and the tropical Pacific mean state. According to our results, a further strengthening of cross-equatorial winds could lead to a suppressed ENSO cycle, but the weakening of these winds will cause more frequent extreme El Niño events.

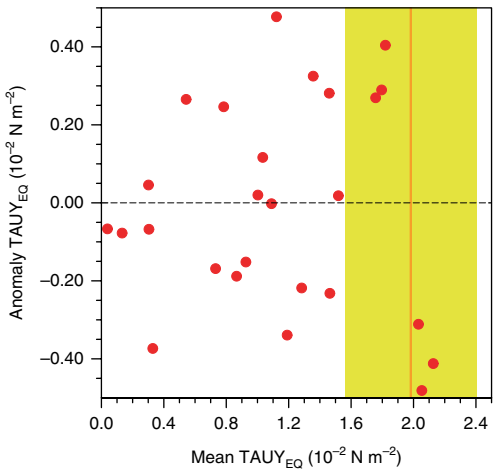

Fig. 4 | Cross-equatorial winds and their projected changes (RCP8.5 (2066–2095) minus historical (1971–2000)) in CMIP5 models. Future anomalies versus modern values of equatorial meridional wind stress ($TAUY_{EQ}$) averaged within the Niño3 box as simulated by CMIP5 models (red dots (Methods)). A 30 yr period of the historical runs (1971–2000) was used to compute the modern values, and another 30 yr period of the RCP8.5 runs (2066–2095) was used to compute the anomalies with respect to the modern values. The orange line indicates the observed strength of the mean cross-equatorial wind stress (for the period 1982–2011 of the ERA-Interim reanalysis). Yellow shading highlights the recent trend in the cross-equatorial winds (+0.008 N m^{-2} over three decades).

Methods

Methods, including statements of data availability and any associated accession codes and references, are available at https://doi.org/10.1038/s41558-018-0248-0.

Received: 19 December 2017; Accepted: 13 July 2018;
Published online: 6 August 2018

References

1. Ashok, K., Behera, S. K., Rao, S. A., Weng, H. Y. & Yamagata, T. El Niño Modoki and its possible teleconnection. *J. Geophys. Res. Oceans* **112**, C11007 (2007).
2. Kao, H. Y. & Yu, J. Y. Contrasting eastern-Pacific and central-Pacific types of ENSO. *J. Clim.* **22**, 615–632 (2009).
3. Kug, J. S., Jin, F. F. & An, S. I. Two types of El Niño events: cold tongue El Niño and warm pool El Niño. *J. Clim.* **22**, 1499–1515 (2009).
4. Yeh, S. W. et al. El Niño in a changing climate. *Nature* **461**, 511–514 (2009).
5. McPhaden, M. J., Lee, T. & McClurg, D. El Niño and its relationship to changing background conditions in the tropical Pacific Ocean. *Geophys. Res. Lett.* **38**, L15709 (2011).
6. Fedorov, A. V. & Philander, S. G. Is El Niño changing? *Science* **288**, 1997–2002 (2000).
7. McPhaden, M. J., Zebiak, S. E. & Glantz, M. H. ENSO as an integrating concept in Earth science. *Science* **314**, 1740–1745 (2006).
8. Collins, M. et al. The impact of global warming on the tropical Pacific Ocean and El Niño. *Nat. Geosci.* **3**, 391–397 (2010).
9. Cai, W. et al. Increasing frequency of extreme El Niño events due to greenhouse warming. *Nat. Clim. Change* **4**, 111–116 (2014).
10. Cai, W. et al. ENSO and greenhouse warming. *Nat. Clim. Change* **5**, 849–859 (2015).
11. Capotondi, A. & Sardeshmukh, P. D. Is El Niño really changing? *Geophys. Res. Lett.* **44**, 8548–8556 (2017).
12. Yeh, S. W. et al. ENSO atmospheric teleconnections and their response to greenhouse gas forcing. *Rev. Geophys.* **56**, 185–206 (2018).
13. Hu, S. & Fedorov, A. V. Exceptionally strong easterly wind burst stalling El Niño of 2014. *Proc. Natl Acad. Sci. USA* **113**, 2005–2010 (2016).
14. Levine, A. F. Z. & McPhaden, M. J. How the July 2014 easterly wind burst gave the 2015–2016 El Niño a head start. *Geophys. Res. Lett.* **43**, 6503–6510 (2016).
15. Hu, S. & Fedorov, A. V. The extreme El Niño of 2015–2016: the role of westerly and easterly wind bursts, and preconditioning by the failed 2014 event. *Clim. Dynam.* https://doi.org/10.1007/s00382-017-3531-2 (2017).
16. Puy, M. et al. Influence of westerly wind events stochasticity on El Niño amplitude: the case of 2014 vs. 2015. *Clim. Dynam.* https://doi.org/10.1007/s00382-017-3938-9 (2017).
17. Santoso, A., McPhaden, M. J. & Cai, W. The defining characteristics of ENSO extremes and the strong 2015/16 El Niño. *Rev. Geophys.* **55**, 1079–1129 (2017).
18. England, M. H. et al. Recent intensification of wind-driven circulation in the Pacific and the ongoing warming hiatus. *Nat. Clim. Change* **4**, 222–227 (2014).
19. Capotondi, A. et al. Understanding ENSO Diversity. *Bull. Am. Meteorol. Soc.* **96**, 921–938 (2015).
20. Wittenberg, A. T. Are historical records sufficient to constrain ENSO simulations? *Geophys. Res. Lett.* **36**, L12702 (2009).
21. Xie, S. P. & Philander, S. G. H. A coupled ocean-atmosphere model of relevance to the ITCZ in the Eastern Pacific. *Tellus A* **46**, 340–350 (1994).
22. Li, X., Xie, S. P., Gille, S. T. & Yoo, C. Atlantic-induced pan-tropical climate change over the past three decades. *Nat. Clim. Change* **6**, 275–279 (2016).
23. Enfield, D. B., Mestas-Nuñez, A. M. & Trimble, P. J. The Atlantic multidecadal oscillation and its relation to rainfall and river flows in the continental US. *Geophys. Res. Lett.* **28**, 2077–2080 (2001).
24. Chiang, J. C. H. & Friedman, A. R. Extratropical cooling, interhemispheric thermal gradients, and tropical climate change. *Ann. Rev. Earth Planet. Sci.* **40**, 383–412 (2012).
25. Frierson, D. M. & Hwang, Y. T. Extratropical influence on ITCZ shifts in slab ocean simulations of global warming. *J. Clim.* **25**, 720–733 (2012).
26. Li, G. & Xie, S. P. Tropical biases in CMIP5 multimodel ensemble: the excessive equatorial Pacific cold tongue and double ITCZ problems. *J. Clim.* **27**, 1765–1780 (2014).
27. Philander, S. G. H. & Pacanowski, R. C. The oceanic response to cross-equatorial winds (with application to coastal upwelling in low latitudes). *Tellus* **33**, 201–210 (1981).
28. Lübbecke, J. F. & McPhaden, M. J. Assessing the twenty-first-century shift in ENSO variability in terms of the Bjerknes stability index. *J. Clim.* **27**, 2577–2587 (2014).
29. Timmermann, A. et al. The influence of a weakening of the Atlantic meridional overturning circulation on ENSO. *J. Clim.* **20**, 4899–4919 (2007).
30. Levine, A. F., McPhaden, M. J. & Frierson, D. M. The impact of the AMO on multidecadal ENSO variability. *Geophys. Res. Lett.* **44**, 3877–3886 (2017).
31. Cheng, W., Chiang, J. C. H. & Zhang, D. X. Atlantic Meridional Overturning Circulation (AMOC) in CMIP5 Models: RCP and historical simulations. *J. Clim.* **26**, 7187–7197 (2013).
32. Rahmstorf, S. et al. Exceptional twentieth-century slowdown in Atlantic Ocean overturning circulation. *Nat. Clim. Change* **5**, 475–480 (2015).
33. Sevellec, F., Fedorov, A. V. & Liu, W. Arctic sea-ice decline weakens the Atlantic Meridional Overturning Circulation. *Nat. Clim. Change* **7**, 604–610 (2017).
34. Xie, S. P. et al. Global warming pattern formation: sea surface temperature and rainfall. *J. Clim.* **23**, 966–986 (2010).
35. Wang, H., Xie, S. P., Tokinaga, H., Liu, Q. & Kosaka, Y. Detecting cross-equatorial wind change as a fingerprint of climate response to anthropogenic aerosol forcing. *Geophys. Res. Lett.* **43**, 3444–3450 (2016).

Acknowledgements

This research was supported by grants to A.V.F. from the NSF (AGS- 0163807) and NASA (NNX17AH21G). S.H. was supported by a NASA Earth and Space Sciences Graduate Fellowship, and a Scripps Institutional Postdoctoral Fellowship. We also acknowledge computational support from the Yale University Faculty of Arts and Sciences High Performance Computing facility and from the NSF/NCAR Yellowstone Supercomputing Center.

Author contributions

S.H. and A.V.F. contributed equally to designing the research and writing the manuscript. S.H. performed the data analysis and numerical simulations and, together with A.V.F., interpreted the results.

Competing interests

The authors declare no competing interests.

Additional information

Supplementary information is available for this paper at https://doi.org/10.1038/s41558-018-0248-0.

Reprints and permissions information is available at www.nature.com/reprints.

Correspondence and requests for materials should be addressed to S.H.

Publisher's note: Springer Nature remains neutral with regard to jurisdictional claims in published maps and institutional affiliations.

Methods

Observational data sets. For SST, we used the National Oceanic and Atmospheric Administration (NOAA) Optimum Interpolation (OI) SST v2 provided the by NOAA Earth System Research Laboratory Physical Sciences Division (http://www.esrl.noaa.gov/psd/data). For wind vector and wind stress products, we used the ERA-Interim reanalysis developed by the European Centre for Medium-Range Weather Forecasts. For precipitation, we used the Global Precipitation Climatology Project v2.2 combined precipitation data set. All these products have a temporal coverage for 1982–2015 and a monthly resolution; a 30 yr period (1982–2011) was used to compute the climatology.

For wind vectors, we compared the ERA-Interim data with the satellite-based NOAA National Climatic Data Center sea winds product and in situ observations from the Tropical Atmosphere Ocean array. All these wind products show consistent results for the strengthening of cross-equatorial winds in the recent decades (Fig. 1). Note that these two data sets use a slightly different period (1995–2005) to compute the climatology, but this does not affect the long-term trends.

Definitions of key variables. To examine the variability and trend of cross-equatorial winds quantitatively, we defined a monthly wind index, V_{EP}, as the surface meridional wind anomalies averaged within the eastern equatorial Pacific (10° S to 10° N and 150–90° W). Our main conclusions do not change if a different equatorial band, for example, 5° S to 5° N, is chosen. We defined a monthly index of local meridional SST gradient, T_{EPy}, by calculating the difference of SST anomalies between the northern (0–10° N and 150–90° W) and the southern (0–10° S and 150–90° W) boxes. The Niño3 index was defined as the SST anomalies averaged within 5° S to 5° N and 150–90° W. All climate indices were low-pass filtered with 11-month running means before conducting the correlation and regression analyses presented in Fig. 2.

Following recent studies[36,37], we defined a heat centre index (HCI) to characterize an average location of El Niño anomalies using equation (1):

$$\mathrm{HCI} = \frac{\int x\mathrm{SSTA}(x)\mathrm{d}x}{\int \mathrm{SSTA}(x)\mathrm{d}x} \quad (1)$$

For each El Niño event, we first averaged SST anomalies (SSTA) within 5° S to 5° N for each longitude (x) within 160–90° W, and then computed the SSTA-weighted longitude after zeroing out all the negative values. The results are presented in Supplementary Fig. 9.

We also calculated the relative frequency of occurrence of CP and EP El Niño events in our simulations. We first defined El Niño events with the November–December–January Niño3.4 index that exceeded one standard deviation. We then identified the location of the maximum SST anomaly and classified the event as CP (EP) if the maximum location was to the west (east) of 150° W, which is the boundary between the Niño3 and Niño4 boxes. We found that the ratio of CP to EP events is 1.2 for the CTL run (55% CP versus 45% EP), and 1.8 for the CrE run (64% CP versus 36% EP). Thus, the strengthening of the cross-equatorial winds increases the ratio of CP to EP events by about a half.

GCM. In this study, we used a climate GCM developed by the National Center for Atmospheric Research, CESM version 1.0.6, in a high-resolution configuration (1.9×2.5 for the atmospheric component, and gx1v6 for the oceanic component)[38,39].

Coupled climate simulations. CESM, just as other state-of-the-art coupled GCMs, has persistent SST and precipitation biases in the tropical Pacific mean state, especially when the seasonal cycle is considered (Supplementary Figs. 6 and 7). The model biases include the so-called double ITCZ problem, which strongly affects cross-equatorial winds. To avoid the potential impacts of such biases, we corrected the model mean state and seasonal SST biases in the tropical Pacific in CESM but maintained the model's interannual variability[40,41]. First, we applied a restoring surface heat flux with a relaxation timescale of 10 d towards the climatological SST based on the 1982–2011 period. The simulation was integrated for 100 years, and then we computed the average monthly restoring heat flux over the last 80 years. Next, we applied this seasonally varying surface heat flux to the original preindustrial run, which modified simulation was then used as the CTL. To detect robust changes in ENSO[20,42], both the CTL and the perturbed simulations described below were integrated for 520 years, and the last 500 years were used for the analysis.

The new CTL has much smaller mean state and seasonal SST biases than the original run, so that the biases in the seasonal evolution of cross-equatorial winds and the ITCZ are greatly reduced (Supplementary Figs. 6 and 7). The flux-adjusted pre-industrial run also simulates a realistic ENSO in periodicity, amplitude and non-linearity (that is, El Niño tends to be stronger than La Niña (Supplementary Fig. 7)).

We next conducted a perturbation experiment, called CrE, by superimposing the observed cross-equatorial wind stress anomaly onto the CTL run; to isolate the dynamic impacts of cross-equatorial winds, we superimposed only the momentum flux and did not modify directly the wind velocity in the atmosphere. To compute the anomaly, first we estimated multidecadal trends in the meridional surface wind stress, which are dominated by positive values (that is, northward trends) in the tropical Pacific (30° S to 15° N and 170–70° W). We then multiplied these local trends by three decades while retaining their spatial structure; the magnitude of the obtained wind stress anomaly was about 40% of the mean meridional wind stress in CTL or the observations. The anomaly was linearly tapered off within an outer 3° buffer zone to avoid sharp changes and then superimposed in the model. To emphasize the impacts of the cross-equatorial wind strengthening, we used only positive values. In addition, sensitivity runs were conducted in which we varied the meridional extent of the superimposed winds, which gave generally similar results.

We further conducted one additional sensitivity run to explore how the Pacific cross-equatorial wind changes can be forced from outside the equatorial Pacific. Specifically, we imposed a warm SST anomaly in the tropical North Atlantic (0–30° N) by restoring the model mixed-layer temperature with a relaxation timescale of 10 d to a target temperature higher than that of the model climatology. The magnitude and spatial structure of the imposed warming follows the observed trends in the Atlantic multiplied by three decades, to yield an anomaly of 0.52 °C (if spatially averaged). The forcing is linearly tapered off within an outer 3° buffer zone to avoid sharp changes. Again, we ran the simulations for 520 years, and investigated the system response after excluding the first 20 years.

We found that this 0.52 °C tropical North Atlantic warming can strengthen the Pacific cross-equatorial winds by 0.40 m s^{-1}. Based on a simple linear scaling, this suggests that the observed tropical North Atlantic warming trend of 0.19 °C dec^{-1} could therefore induce a cross-equatorial wind strengthening of 0.15 m s^{-1} dec^{-1}. For comparison, this is about two-thirds of the full V_{EP} trend (0.22 m s^{-1} dec^{-1}) in the observations (the full trend accounts for all the factors, and include the contribution from the observed local meridional SST dipole). Our results suggest that a cross-equatorial wind strengthening could, indeed, be forced from outside the tropical Pacific.

We also investigated the ENSO response to the tropical Atlantic warming. We found that ENSO variability is significantly reduced, particularly in the eastern Pacific, consistent with our main experiment CrE in which cross-equatorial winds were directly imposed. Note that the tropical North Atlantic warming induces both zonal and meridional wind changes over the tropical Pacific, which makes it more difficult to separate their impacts. In this study, we predominantly focused on the (meridional) cross-equatorial winds as their role has been largely overlooked previously; a more comprehensive analysis on the impacts of the Atlantic will be reported elsewhere.

Mixed-layer heat-budget analysis. To better understand the mechanisms of how cross-equatorial winds weaken the ENSO variability, we conducted a mixed-layer heat-budget analysis[3,17] for El Niño composites in both simulations (CTL and CrE). The heat-budget equation is:

$$\begin{aligned} T'_t = & -[(u'\bar{T}_x + \bar{u}T'_x + u'T'_x) + \left(v'\bar{T}_y + \bar{v}T'_y + v'T'_y\right) \\ & + (w'\bar{T}_z + \bar{w}T'_z + w'T'_z)] + Q' + R \end{aligned} \quad (2)$$

where Q is the surface net heat flux. We only focus on advective terms and air–sea heat fluxes here, and all the rest is accounted for in the residual R. First, for each simulation, we constructed composites of El Niño, defined when the November–December–January Niño3.4 index (that is, SST anomalies averaged within 5° S to 5° N and 170–120° W) exceeded its standard deviation. We then computed each term in the heat-budget equation and computed averages within the Niño3 box (5° S to 5° N and 150–90° W) in the upper ocean (50 m) during the development of El Niño events (April–December). The results are presented in Supplementary Fig. 10, where each advective term shown has incorporated its negative sign as is shown in equation (2).

Coupled Model Intercomparison Project Phase 5 (CMIP5) model analysis. We examined changes in the cross-equatorial winds in 26 climate models from CMIP5[43] available online (https://cmip.llnl.gov/cmip5/). We chose the 1971–2000 interval in historical simulations and 2066–2095 in RCP8.5 simulations for the analysis. The 26 climate models are CanESM2, CCSM4, CMCC-CESM, CMCC-CM, CMCC-CMS, CNRM-CM5, GFDL-CM3, GFDL-ESM2G, GFDL-ESM2M, GISS-E2-H, GISS-E2-H-CC, GISS-E2-R-CC, HadGEM2-AO, HadGEM2-CC, HadGEM2-ES, inmcm4, IPSL-CM5A-LR, IPSL-CM5A-MR, IPSL-CM5B-LR, MIROC5, MIROC-ESM, MIROC-ESM-CHEM, MRI-CGCM3, MRI-ESM1, NorESM1-M and NorESM1-ME. The results are presented in Fig. 4 and discussed in the main text.

Data availability. The NOAA OI SST product is publicly available at https://www.esrl.noaa.gov/psd/data/gridded/data.noaa.oisst.v2.highres.html. The Global Precipitation Climatology Project precipitation product is publicly available at https://www.esrl.noaa.gov/psd/data/gridded/data.gpcp.html. The ERA interim wind product is publicly available at https://www.ecmwf.int/en/forecasts/datasets/archive-datasets/reanalysis-datasets/era-interim. The NOAA National Climatic Data Center wind product is publicly available at https://www.ncdc.noaa.gov/data-access/marineocean-data/blended-global/blended-sea-winds. The Tropical Atmosphere Ocean array wind product is publicly available at https://www.pmel.noaa.gov/tao/drupal/disdel/. The CMIP5 data sets are publicly available at https://cmip.llnl.gov/cmip5/. The data that support the findings of this study are available from the corresponding author upon request.

References

36. Giese, B. S. & Ray, S. El Niño variability in simple ocean data assimilation (SODA), 1871–2008. *J. Geophys. Res. Oceans* **116**, C02024 (2011).
37. Fedorov, A. V., Hu, S. N., Lengaigne, M. & Guilyardi, E. The impact of westerly wind bursts and ocean initial state on the development, and diversity of El Niño events. *Clim. Dynam.* **44**, 1381–1401 (2015).
38. Deser, C. et al. ENSO and Pacific decadal variability in the Community Climate System Model Version 4. *J. Clim.* **25**, 2622–2651 (2012).
39. Capotondi, A. ENSO diversity in the NCAR CCSM4 climate model. *J. Geophys. Res. Oceans* **118**, 4755–4770 (2013).
40. Manabe, S. & Stouffer, R. J. Two stable equilibria of a coupled ocean–atmosphere model. *J. Clim.* **1**, 841–866 (1988).
41. Liu, W., Liu, Z. Y. & Brady, E. C. Why is the AMOC monostable in coupled general circulation models? *J. Clim.* **27**, 2427–2443 (2014).
42. Vega-Westhoff, B. & Sriver, R. L. Analysis of ENSO's response to unforced variability and anthropogenic forcing using CESM. *Sci. Rep.* **7**, 18047 (2017).
43. Taylor, K. E., Stouffer, R. J. & Meehl, G. A. An overview of CMIP5 and the experiment design. *Bull. Am. Meteorol. Soc.* **93**, 485–498 (2012).